

# Configurational temperature in active-matter models

Shibu Saw, Lorenzo Costigliola, and Jeppe C. Dyre\*  
*Glass and Time, IMFUFA, Department of Science and Environment,  
Roskilde University, P.O. Box 260, DK-4000 Roskilde, Denmark*  
(Dated: May 23, 2022)

**Abstract:** We show that the liquid-state-theory configurational temperature  $T_{\text{conf}}$  defines an energy scale, which for active-matter models of point particles based on a potential-energy function can be used to determine how to adjust model parameters to achieve approximately invariant structure and dynamics when the density is changed. The required parameter changes are calculated from the variation of a single configuration's  $T_{\text{conf}}$  upon a uniform scaling of all coordinates. The formalism developed applies for models involving a potential-energy function with hidden scale invariance. The procedure is illustrated by computer simulations of the Kob-Andersen binary Lennard-Jones model with active Ornstein-Uhlenbeck dynamics in three dimensions and the two-dimensional single-component Yukawa model with active Brownian particle dynamics. For the latter model we also show how  $T_{\text{conf}}$  may be applied for estimating the MIPS phase boundary, in effect reducing by one the dimension of the parameter space. We finally propose that the ratio between the equilibrium-system temperature corresponding to actual potential energy and  $T_{\text{conf}}$  provides a useful measure of how far an active-matter system is from thermal equilibrium.

arXiv:2204.06819v2 [cond-mat.soft] 20 May 2022

---

\* dyre@ruc.dk

## I. INTRODUCTION

Any system in thermal equilibrium has a well-defined temperature, and temperature is fundamental in thermodynamics and statistical mechanics. In view of this it is obvious to try to generalize the concept of temperature to non-equilibrium systems. Excellent reviews of different temperatures that have been proposed throughout the years are given in Refs. 1–5. Examples are the *effective temperature* quantifying deviations from the fluctuation-dissipation theorem [6–8] and the *fictive temperature* characterizing a glass’ structure in terms of the temperature at which the liquid solidified [9, 10]. Non-equilibrium temperatures are generally motivated by the prospect of connecting the non-equilibrium system in question to thermal-equilibrium properties of the same system. That is not the motivation, however, of the below proposed application of liquid-state theory’s *configurational temperature* [2, 11–13] to active-matter models, which instead focuses on scaling properties.

Active matter is an umbrella term used to describe any physical system whose building blocks can autonomously perform mechanical work. This includes fluids consisting of self-propelled particles (e.g., Quincke rollers, suspensions of swimming bacteria, animal groups), mutually-propelled particles (e.g., cytoskeletal filaments and motor proteins), immobile dividing cells (e.g., sessile bacteria), immobile contractile cells (e.g., epithelia), etc. A common theme of active matter is the self propulsion as found, e.g., in connection with cell migration, bacterial motion, and bird or insect flock dynamics [14–21]. Active matter is not time reversible (although in some instances like that of active turbulence there may be statistically time-reversible states). This means that a multitude of different dynamics may come into play [22], presenting a much richer field of study than that of ordinary time-reversible dynamics [23]. A noted example of the intriguing features of active matter is motility-induced phase separation (MIPS), which is the finding that even a purely repulsive system may phase separate into high- and low-density phases [17, 19, 24–28].

Active matter does not have states of ordinary thermal equilibrium, but there have been suggestions for how to map active-matter states to equilibrium, implying the existence of a non-equilibrium active-matter temperature. For instance, Szamel proposed an effective temperature for a single self-propelled particle [29], and Fodor *et al.* showed [30] that for active Ornstein-Uhlenbeck particles (AOUP) at small persistence time one can identify an effective temperature from the analog of the fluctuation-dissipation theorem (see also Refs. 31–33). In a parallel development, Takatori and Brady formulated a thermodynamic-type temperature for active matter based on the swim-pressure concept [34].

For an ordinary time-reversal-invariant system in thermal equilibrium, the temperature  $T$  is equal to  $T_{\text{conf}}$  that is defined [2, 12] as follows. For a system of  $N$  particles with collective coordinate vector  $\mathbf{R} \equiv (\mathbf{r}_1, \dots, \mathbf{r}_N)$  and potential-energy function  $U(\mathbf{R})$ ,  $k_B T_{\text{conf}} \equiv \langle (\nabla U)^2 \rangle / \langle \nabla^2 U \rangle$  in which  $k_B$  is the Boltzmann constant,  $\nabla$  is the gradient operator in the  $3N$ -dimensional configuration space, and the sharp brackets denote canonical-ensemble averages. The proof that  $T_{\text{conf}} = T$  in equilibrium is so simple that it deserves to be repeated here [11]: If  $Z$  is the configuration-space partition integral, a partial integration of  $\langle \nabla^2 U \rangle = \int \nabla^2 U(\mathbf{R}) \exp(-U(\mathbf{R})/k_B T) d\mathbf{R} / Z$  leads to  $\langle \nabla^2 U \rangle = - \int \nabla U(\mathbf{R}) \cdot \nabla \exp(-U(\mathbf{R})/k_B T) d\mathbf{R} / Z = \langle (\nabla U)^2 \rangle / k_B T$  from which  $T_{\text{conf}} = T$  follows.

Approaching the thermodynamic limit, the relative fluctuations of both the numerator and the denominator of  $T_{\text{conf}}$  vanish. This means that if one defines an  $\mathbf{R}$ -dependent configurational temperature by

$$k_B T_{\text{conf}}(\mathbf{R}) \equiv \frac{(\nabla U(\mathbf{R}))^2}{\nabla^2 U(\mathbf{R})}, \quad (1)$$

the identity  $T_{\text{conf}}(\mathbf{R}) \cong T$  applies in the sense that deviations vanish as  $N \rightarrow \infty$ . We have this limit in mind throughout and shall (mostly) ignore that  $T_{\text{conf}}(\mathbf{R})$  fluctuates slightly for any finite system. Note that, in contrast to the “standard” kinetic-energy based temperature definition, the configurational temperature is not defined for a system of free particles. Note also that configurations with  $\nabla^2 U(\mathbf{R}) = 0$  become less likely as  $N \rightarrow \infty$  so the fact that Eq. (1) is not defined for such configurations is irrelevant; by the same argument one can ignore the existence of configurations with  $\nabla^2 U(\mathbf{R}) < 0$ . We return below briefly to a discussion of  $T_{\text{conf}}$  fluctuations in simulations (Fig. 3). Finally, we note that the focus of the present paper is on the subset of active-matter models without orientational interactions.

Since the derivation of the configurational temperature  $T_{\text{conf}}$  is based on the fact that the probability in the canonical ensemble of configuration  $\mathbf{R}$  is proportional to  $\exp(-U(\mathbf{R})/k_B T)$ , it would appear that  $T_{\text{conf}}$  cannot be relevant for systems that are far from thermal equilibrium. We show below that  $T_{\text{conf}}(\mathbf{R})$  may nevertheless be used for tracing out lines of invariant structure and dynamics in the phase diagram of certain active-matter models with hidden scale invariance. The latter is the symmetry that the ordering of configurations according to their potential energy at a given density is maintained if these are scaled uniformly to a different density (compare Eq. (6) below), a property that applies to a good approximation for a number of well-known pair potentials, including the Lennard-Jones and Yukawa interaction [35–38].

## II. APPROXIMATELY INVARIANT PHYSICS AT DIFFERENT DENSITIES OF THE KOB-ANDERSEN AOUP MODEL

This section studies the active Ornstein-Uhlenbeck particle (AOUP) dynamics of the Kob-Andersen (KA) binary Lennard-Jones (LJ) model [39], which is popular in numerical studies of viscous liquids and the glass transition because it is easily supercooled into a metastable highly viscous liquid state [40]. We simulated a KA system of 10000 particles consisting of two spheres, A (80%) and B (20%). Writing the LJ pair potential between particles of type  $\alpha$  and  $\beta$  as  $v_{\alpha\beta}(r) = 4\varepsilon_{\alpha\beta}((r/\sigma_{\alpha\beta})^{-12} - (r/\sigma_{\alpha\beta})^{-6})$  with  $\alpha, \beta = A, B$ , the KA parameters are [39]  $\sigma_{AA} = 1.0$ ,  $\sigma_{AB} = \sigma_{BA} = 0.8$ ,  $\sigma_{BB} = 0.88$ ,  $\varepsilon_{AA} = 1.0$ ,  $\varepsilon_{AB} = \varepsilon_{BA} = 1.5$ ,  $\varepsilon_{BB} = 0.5$ . A shifted-force cutoff of  $v_{\alpha\beta}(r)$  at  $r_{\text{cut}} = 2.5\sigma_{\alpha\beta}$  was used [41]. The simulations employed the time step  $\Delta t = \Delta\tilde{t}/(D\rho^{2/3})$  in which  $\Delta\tilde{t} = 0.4$  and  $\rho$  is the (particle) density. At the reference density  $\rho = 1.2$  the value of  $\Delta t = 0.0001$  was used. The simulations were carried out on GPU cards, with the active-matter simulations using a home-made code while the MD simulations used RUMD [42].

The AOUP model is a model which has no momentum conservation and for which hydrodynamics is not taken into account; all information about particle interactions is contained in the potential-energy function [15, 20, 43]. In the  $3N$ -dimensional configuration space the AOUP equation of motion [30, 44–46] is

$$\dot{\mathbf{R}} = \mu\mathbf{F}(\mathbf{R}) + \boldsymbol{\eta}(t). \quad (2)$$

Here  $\mu$  is the mobility (velocity over force) and the force vector is given by  $\mathbf{F}(\mathbf{R}) = -\nabla U(\mathbf{R})$ . The noise vector  $\boldsymbol{\eta}(t)$  is colored according to an Ornstein-Uhlenbeck process, i.e., is a Gaussian stochastic process characterized by

$$\langle \eta_i^\alpha(t)\eta_j^\beta(t') \rangle = \delta_{ij}\delta_{\alpha\beta} \frac{D}{\tau} e^{-|t-t'|/\tau} \quad (3)$$

in which  $i$  and  $j$  are particle indices,  $\alpha$  and  $\beta$  represent spatial  $xyz$  indices, and  $D$  and  $\tau$  are constants. The diffusion coefficient  $D$  is that of a single AOUP, which may be used to introduce a single-particle effective temperature. We are interested in how the physics is affected when the density is changed. The question addressed below is whether approximately invariant physics can be obtained by adjusting  $D$  and  $\tau$  (regarding  $\mu$  as a material constant throughout) in the sense that a movie of the particle motion will show the same except for a scaling of space and time.

The dimension of  $\mu$  is length squared over energy times time. Thus, if  $l_0$  is a length unit,  $t_0$  a time unit, and  $e_0$  an energy unit, the quantity  $\mu(t_0e_0/l_0^2)$  is dimensionless. Likewise,  $D(t_0/l_0^2)$  and  $\tau/t_0$  are dimensionless because  $D$  has the dimension of a diffusion coefficient and  $\tau$  of a time. It is reasonable to expect that when the density is changed, invariant physics can come about only if these three dimensionless quantities do not change. As length unit we take the average interparticle spacing,  $l_0 = \rho^{-1/3}$ . The colored-noise correlation time  $\tau$  of Eq. (3) is a natural choice for the time unit,  $t_0 = \tau$ . The idea is now to investigate the consequences of using for the energy unit the configurational temperature, i.e., choosing  $e_0 = k_B T_{\text{conf}}$  (Sec. III justifies this choice). If the above two dimensionless quantities are to be invariant when density varies, the following must apply:  $\mu \propto l_0^2/(t_0e_0) = \rho^{-2/3}/(\tau k_B T_{\text{conf}})$  and to  $D \propto l_0^2/t_0 = \rho^{-2/3}/\tau$ . Since  $\mu$  is assumed constant, this leads to  $\tau \propto \rho^{-2/3}/k_B T_{\text{conf}}$  and  $D \propto k_B T_{\text{conf}}$ , i.e., the following equations determine  $D$  and  $\tau$  at the density  $\rho$  from their values  $D_0$  and  $\tau_0$  at a reference state point of density  $\rho_0$ ,

$$\begin{aligned} D &= D_0 \frac{T_{\text{conf}}(\rho)}{T_{\text{conf}}(\rho_0)}, \\ \tau &= \tau_0 \left( \frac{\rho_0}{\rho} \right)^{2/3} \frac{T_{\text{conf}}(\rho_0)}{T_{\text{conf}}(\rho)}. \end{aligned} \quad (4)$$

We note that  $D$  scales in proportion to the configurational temperature  $T_{\text{conf}}$ , which is analogous to the equilibrium result  $D \propto T$  where  $T$  is the temperature.

As mentioned, fluctuations are small for a large system, so  $T_{\text{conf}}(\rho_0)$  may be evaluated from a single configuration of a steady-state simulation,  $\mathbf{R}_0$  by means of  $T_{\text{conf}}(\rho_0) \cong T_{\text{conf}}(\mathbf{R}_0)$ . In order to find  $T_{\text{conf}}(\rho)$  one scales  $\mathbf{R}_0$  uniformly to the density  $\rho$  using  $\mathbf{R} = (\rho_0/\rho)^{1/3}\mathbf{R}_0$ ; the configurational temperature is then identified from  $T_{\text{conf}}(\rho) \cong T_{\text{conf}}(\mathbf{R})$ . When substituted into Eq. (4) this leads to the following recipe for calculating  $D$  and  $\tau$  at density  $\rho$

$$\begin{aligned} D &= D_0 \frac{T_{\text{conf}}[(\rho_0/\rho)^{1/3}\mathbf{R}_0]}{T_{\text{conf}}(\mathbf{R}_0)}, \\ \tau &= \tau_0 \left( \frac{\rho_0}{\rho} \right)^{2/3} \frac{T_{\text{conf}}(\mathbf{R}_0)}{T_{\text{conf}}[(\rho_0/\rho)^{1/3}\mathbf{R}_0]}. \end{aligned} \quad (5)$$

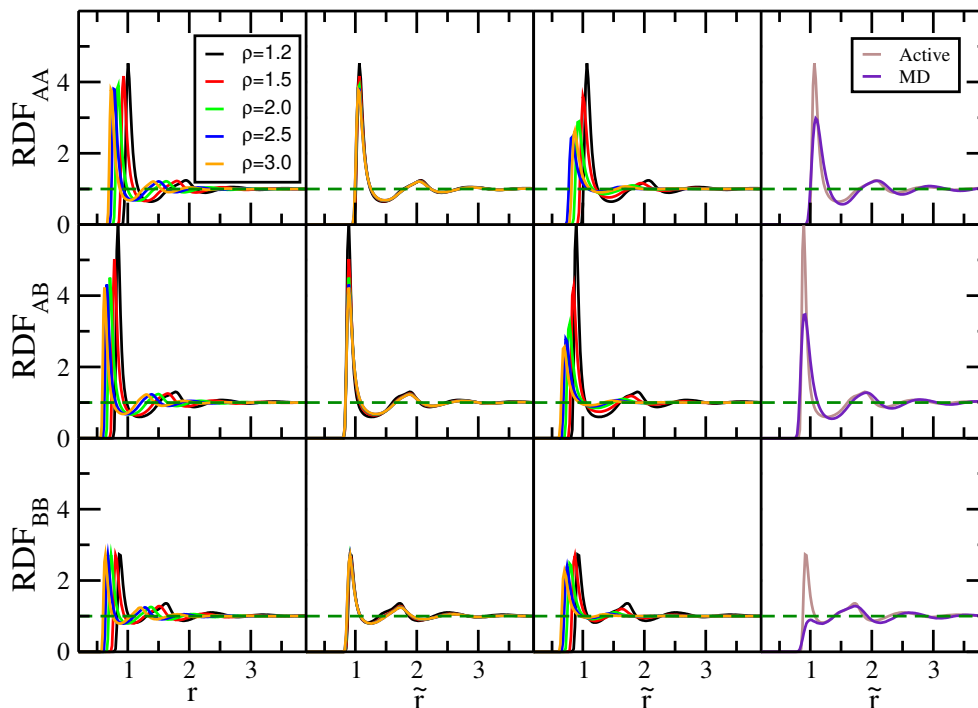


FIG. 1. Radial distribution functions (RDF) of the Kob-Andersen system with active Ornstein-Uhlenbeck (AOUP) dynamics at densities between 1.2 and 3.0 for the model parameters  $D$  and  $\tau$  of Table I determined by means of Eq. (5) and Eq. (1). The first column shows the three partial RDFs along the proposed line of invariance generated from the reference state point  $(\rho_0, D_0, \tau_0) = (1.2, 3000, 10)$ , plotted as functions of the pair distance  $r$ . The second column shows the same data plotted as functions of the reduced pair distance  $\tilde{r} \equiv \rho^{1/3}r$ , revealing a good collapse except at the first peak of  $g_{AB}$ . For comparison, the third column shows data for the same values of  $D$  and  $\tau$  as the two previous columns at the fixed density  $\rho = 1.2$ ; the fourth column shows AOUP data at the reference state point (brown) and standard MD thermal equilibrium data (indigo) at the density  $\rho = 1.2$  and the MD temperature that results in the same average potential energy as that of the AOUP simulation ( $T_{MD} = 1.57$ ).

Table I shows the resulting values of  $D$  and  $\tau$  for densities ranging from 1.2 to 3.0, starting from the reference state point  $(\rho, D, \tau) = (1.2, 3000, 10)$ .

$\rho$	$D$	$\tau$	$T_{\text{conf}}$
1.2	3000	10.000	0.2742
1.5	9859	2.622	0.9014
2.0	39160	0.5450	3.580
2.5	105600	0.1741	9.657
3.0	230800	0.0706	21.10

TABLE I. Density  $\rho$  and model parameters  $D$  and  $\tau$  along the predicted line of invariance calculated from Eq. (5) in which  $T_{\text{conf}}(\rho)$  is determined from a single configuration  $\mathbf{R}_0$  by means of Eq. (1) after first scaling it uniformly to density  $\rho$ .

The two left columns of Fig. 1 show the three partial radial distribution functions (RDFs) along the predicted line of invariance plotted, respectively, as a function of the radial distance  $r$  and of the reduced radial distance  $\tilde{r} \equiv \rho^{1/3}r$ . The latter shows good invariance, except that the height of the first peak is not invariant, in particular for the AB RDF. The third column of Fig. 1 shows the results for the same values of  $D$  and  $\tau$  as previously (see Table I) but with the fixed density  $\rho = 1.2$ , in which case no invariance is observed. Finally, the fourth column compares the reference density RDFs with those of a thermal-equilibrium molecular-dynamics (MD) simulation at the reference density and the temperature at which the average potential energy is equal to that of the reference-state-point AOUP simulation ( $T_{MD} = 1.57$ ), showing little resemblance. This temperature is quite different from the configurational temperature ( $T_{\text{conf}} = 0.27$ , which corresponds to such a deeply supercooled state for the Newtonian system that the metastable

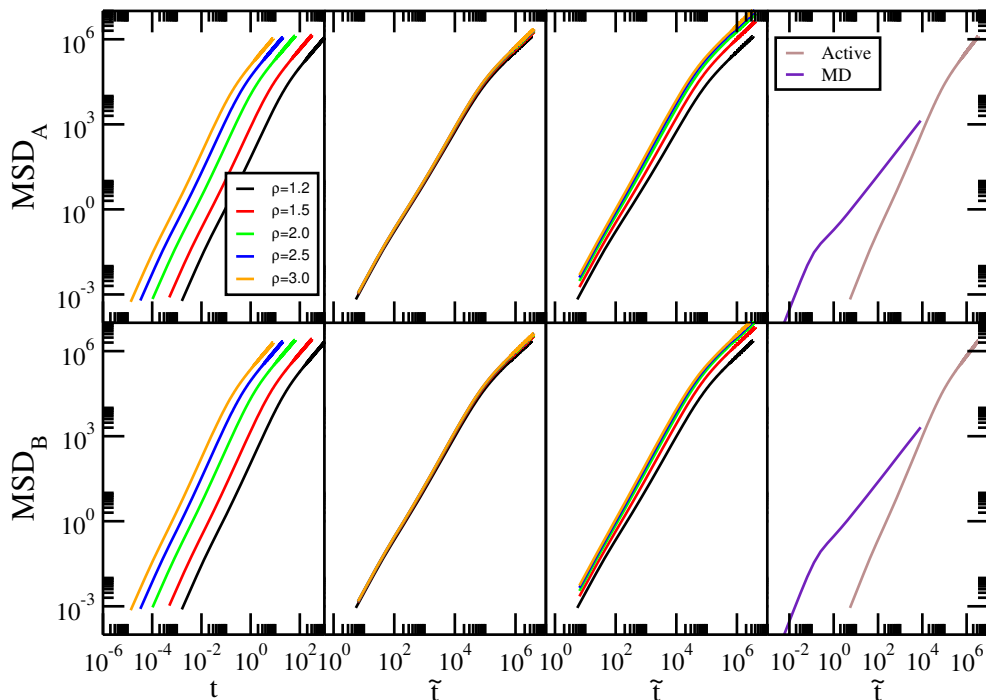


FIG. 2. Mean-square displacement (MSD) at the same state points as in Fig. 1. The first column shows the MSD of the A and B particles along the predicted line of invariance, plotted as a function of the time  $t$ . The second column shows the same data in reduced units revealing a good collapse. The third column shows reduced data for the same values of  $D$  and  $\tau$  as the previous figures at the fixed density  $\rho = 1.2$ . The fourth column shows a comparison of the reduced MSD AOUP data at the reference state point (brown) to standard reduced MD thermal-equilibrium data (indigo) at  $\rho = 1.2$ , where the temperature was determined to result in the same average potential energy as the AOUP simulation ( $T_{MD} = 1.57$ ); the MD reduced units are defined below in Eq. (7).

liquid presently cannot be equilibrated using MD).

Figure 2 shows the mean-square displacement (MSD) of the A and B particles as functions of the time. The four columns are similar to those of Fig. 1 with the time  $t$  as the x-coordinate in the first column and the reduced time  $\tilde{t} \equiv (D\rho^{2/3})t \propto t/\tau$  in the second, where the MSD is also given in reduced units, i.e., multiplied by  $\rho^{2/3}$ . The latter shows approximate invariance of the dynamics. It is instructive to consider the limits of short and long times. For  $t \rightarrow 0$ , in the “ballistic” regime, Eq. (2) and Eq. (3) imply that the MSD is proportional to  $(D/\tau)t^2$ , while for  $t \rightarrow \infty$  the MSD is proportional to  $Dt$ . Thus the reduced-unit short- and long-time limit MSDs are proportional to  $\rho^{2/3}D\tau\tilde{t}^2$  and  $\rho^{2/3}D\tau\tilde{t}$ , respectively. Since Eq. (5) implies that  $\rho^{2/3}D\tau$  is a constant, this means that in these limit the MSDs are simply proportional to  $\tilde{t}^2$  and  $\tilde{t}$ , respectively, which is confirmed by Fig. 2(b). The third column of Fig. 2 gives the reduced MSD using the predicted  $D$  and  $\tau$  at the reference density. The fourth column compares the reference state point MSDs to those of the  $T_{MD} = 1.57$  MD simulation. We conclude from Fig. 1 and Fig. 2 that there is a nontrivial approximate invariance of structure and dynamics.

Figure 3 investigates the robustness of the procedure used for generating lines of approximately invariant structure and dynamics in the general AOUP phase diagram. Figure 3(a) shows  $T_{\text{conf}}$  as a function of  $\rho$  in a log-log plot for selected scaling configuration  $\mathbf{R}_0$  used in Eq. (5). At high density one finds almost  $T_{\text{conf}}(\rho) \propto \rho^4$ , which reflects the dominance here of the  $r^{-12}$  repulsive term of the LJ pair potential – it is straightforward to show from Eq. (1) that  $T_{\text{conf}}(\rho) \propto \rho^{n/3}$  for a system of inverse power-law pair potentials  $\propto r^{-n}$ . At lower densities this does not apply, however, showing that the invariance of structure and dynamics is not a trivial consequence of the scale-invariant repulsive  $r^{-12}$  term of the LJ pair potential. Figure 3(b) shows the distribution of configurational temperatures for the system simulated at the reference state point. We find a fairly broad distribution. This motivates an investigation into how much the prediction of the invariance line depends on the choice of the  $\mathbf{R}_0$ . Figures 3(c) and (d) show the predictions for  $D$  and  $\tau$  using three different configurations in Eq. (1). The red curve is for the scaling configuration  $\mathbf{R}_0$  used above that was selected from the center of the distribution in (b), while the black and blue curves are for two configurations taken from the lower and higher ends of the distribution. For both  $D$  and  $\tau$  there is little visible difference; in the two latter cases we find that the RDFs and MSDs are virtually indistinguishable from those of Fig. 1 and Fig. 2 (data not shown). Only a ratio of configurational temperatures is present in Eq. (5), and it appears that

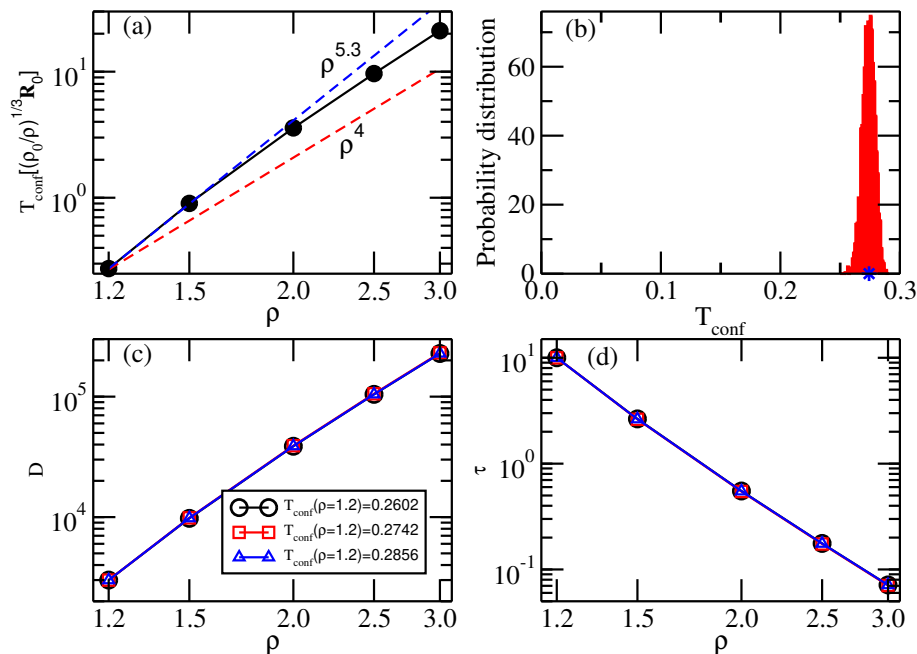


FIG. 3. Configurational temperature variation. (a) shows the configurational temperature  $T_{\text{conf}}$  as a function of the density for the selected scaling configuration  $\mathbf{R}_0$ . At the highest temperatures,  $T_{\text{conf}}$  scales with density in proportion to  $\rho^4$  (red dashed line); this is where the repulsive  $r^{-12}$  term of the LJ pair potential dominates the potential energy. At the lowest temperatures, the scaling is approximately proportional to  $\rho^{5.3}$  (blue dashed line), showing that the scaling is nontrivial. (b) shows the distribution of  $T_{\text{conf}}$  for  $N = 10000$  particles at the reference state point. The spread is much larger than expected from a simple statistical  $1/\sqrt{N}$  argument. The blue star marks  $T_{\text{conf}}$  of the reference scaling configuration  $\mathbf{R}_0$ . (c) shows how  $D$  varies according to Eq. (5) for three different configurations: one is the  $\mathbf{R}_0$  used in Fig. 1 and Fig. 2, which was selected from the center of the distribution (red), the two others are from the lowest and highest ends of the distribution (black and blue). (d) shows how  $\tau$  varies according to Eq. (5) for the same three configurations.

a significant cancellation occurs. This means that, despite the relatively large spread of  $T_{\text{conf}}$ ,  $N = 10000$  particles are enough for Eq. (4) to be used for predicting model parameters resulting in approximately invariant structure and dynamics.

### III. JUSTIFICATION OF THE PROCEDURE

How can the canonical-ensemble-based characteristic energy  $k_B T_{\text{conf}}$  provide the relevant energy scale for identifying invariant active-matter physics upon a density change? While the energy  $k_B T_{\text{conf}}$  *per se* may not have physical relevance in active-matter models, we argue below that the ratio  $T_{\text{conf}}(\rho)/T_{\text{conf}}(\rho_0)$  determines the ratio of the relevant energy scales at the two densities. To arrive at this conclusion, it is necessary to first summarize some recent findings.

The starting point is that the KA model to a good approximation obeys the hidden-scale-invariance symmetry defined [36, 38] by the following logical implication for the potential-energy function  $U(\mathbf{R})$ ,

$$U(\mathbf{R}_a) < U(\mathbf{R}_b) \Rightarrow U(\lambda \mathbf{R}_a) < U(\lambda \mathbf{R}_b). \quad (6)$$

Here  $\mathbf{R}_a$  and  $\mathbf{R}_b$  are configurations of the same density and  $\lambda$  is a uniform-scaling parameter. Physically, Eq. (6) expresses that the ordering of configurations at one density according to their potential energy is maintained when configurations are scaled uniformly to a different density. At a given thermodynamic equilibrium state point, the excess entropy  $S_{\text{ex}}$  is defined as the entropy minus the ideal-gas entropy at the same density and temperature [47]. In the case of ordinary Newtonian mechanics, Eq. (6) implies that structure and dynamics in reduced units (see below) are invariant along the curves of constant excess entropy [35, 36, 38]. These curves are termed isomorphs, and systems with isomorphs are termed R-simple.

Isomorph invariance is exact whenever Eq. (6) applies without exception, but this is never the case for pair potentials with both attractions and repulsions. Isomorph invariance is still a good approximation, however, if Eq. (6) applies for

most of the physically relevant configurations at the state points in question. This is believed to be the case for most metals and van der Waals bonded systems, whereas systems with strong directional interactions like hydrogen-bonded and covalently bonded systems generally do not conform to Eq. (6) and violate isomorph-theory predictions [48] (ionic and dipolar systems constitute a class in-between). Realistic pair-potential models with approximate hidden scale invariance include the standard Lennard-Jones model in single-component, binary, and polydisperse versions and with exponents other than 6 and 12 (the so-called Mie potentials), as well as the Yukawa (screened Coulomb) pair potential [36, 49]. For systems with inverse-power-law interactions, isomorph theory is exact.

For R-simple systems with Newtonian dynamics, the structure and dynamics of the condensed liquid and solid phases are isomorph invariant to a good approximation when made dimensionless using as “reduced” units the length  $l_0$ , energy  $e_0$ , and time  $t_0$  given by (where  $m$  is the particle mass)

$$l_0 = \rho^{-1/3}, \quad e_0 = k_B T, \quad t_0 = \rho^{-1/3} \sqrt{m/k_B T}. \quad (7)$$

The microscopic excess entropy is defined [36] by  $S_{\text{ex}}(\mathbf{R}) \equiv S_{\text{ex}}(\rho, U(\mathbf{R}))$  in which  $S_{\text{ex}}(\rho, U)$  is the thermodynamic excess entropy of the equilibrium state point with density  $\rho$  and average potential energy  $U$ . Note that the function  $S_{\text{ex}}(\mathbf{R})$  is defined for any configuration of any system, whether R-simple or not. It can be shown that if Eq. (6) applies, however,  $S_{\text{ex}}(\mathbf{R})$  depends only on the configuration’s reduced coordinates,  $\tilde{\mathbf{R}} \equiv \rho^{1/3} \mathbf{R}$  [36]. Inverting the relation  $S_{\text{ex}}(\mathbf{R}) = S_{\text{ex}}(\rho, U(\mathbf{R}))$  for an R-simple system thus leads to

$$U(\mathbf{R}) = U(\rho, S_{\text{ex}}(\tilde{\mathbf{R}})) \quad (8)$$

in which  $U(\rho, S_{\text{ex}})$  is the average potential energy of the thermodynamic equilibrium state point with density  $\rho$  and excess entropy  $S_{\text{ex}}$ .

Consequences of Eq. (8) have so far been worked out only for systems with standard time-reversible Newtonian dynamics [36, 38], but since Eq. (8) follows from Eq. (6) that has no reference to thermal equilibrium, Eq. (8) may also be applied to active-matter models with a hidden-scale-invariant potential-energy function. Note that the function  $S_{\text{ex}}(\mathbf{R})$  still refers to the standard microcanonical ensemble according to which  $S_{\text{ex}}(\mathbf{R})$  is basically the logarithm of the number of configurations with the same density and potential energy as  $\mathbf{R}$  [36].

We proceed to rewrite the AOUP equation of motion in terms of dimensionless variables. Writing  $\mathbf{R} = l_0 \tilde{\mathbf{R}}$  and  $t = t_0 \tilde{t}$  in which  $l_0 = \rho^{-1/3}$  and  $t_0 = \tau$  as in Sec. II, Eq. (2) becomes (in which  $\tilde{\nabla} = \rho^{-1/3} \nabla$ )

$$\frac{l_0}{\tau} \dot{\tilde{\mathbf{R}}} = -\mu \frac{1}{l_0} \tilde{\nabla} U(\mathbf{R}) + \boldsymbol{\eta}(\tilde{t}). \quad (9)$$

The reduced noise is given by  $\tilde{\boldsymbol{\eta}} = (\tau/l_0) \boldsymbol{\eta}$  in terms of which Eq. (3) becomes

$$\langle \tilde{\eta}_i^\alpha(\tilde{t}) \tilde{\eta}_j^\beta(\tilde{t}') \rangle = \delta_{ij} \delta_{\alpha\beta} \frac{\tau D}{l_0^2} e^{-|\tilde{t}-\tilde{t}'|}. \quad (10)$$

Equation (9) leads to

$$\dot{\tilde{\mathbf{R}}} = -\mu \frac{\tau}{l_0^2} \tilde{\nabla} U(\mathbf{R}) + \tilde{\boldsymbol{\eta}}(\tilde{t}). \quad (11)$$

For any configuration  $\mathbf{R}$  the systemic temperature  $T_s(\mathbf{R})$  is defined [50] by

$$T_s(\mathbf{R}) \equiv \left( \frac{\partial U}{\partial S_{\text{ex}}} \right) \Big|_{\rho, S_{\text{ex}}=S_{\text{ex}}(\mathbf{R})}. \quad (12)$$

In a steady-state situation the fluctuations of the systemic temperature go to zero in the thermodynamic limit, just as those of  $T_{\text{conf}}(\mathbf{R})$ . We henceforth often leave out  $\mathbf{R}$  when convenient and write simply  $T_s$ . In practice, to determine  $T_s(\mathbf{R})$  one utilizes the fact that  $T_s(\mathbf{R})$  is the equilibrium temperature  $T_{\text{eq}}$  of the thermodynamic state point with the density of  $\mathbf{R}$  and excess entropy  $S_{\text{ex}}(\mathbf{R})$ , implying that [50]

$$T_s(\mathbf{R}) = T_{\text{eq}}(\rho, S_{\text{ex}}(\tilde{\mathbf{R}})) = T_{\text{eq}}(\rho, U(\mathbf{R})). \quad (13)$$

Equation (8) leads to  $\tilde{\nabla}U(\mathbf{R}) = T_s \tilde{\nabla}S_{\text{ex}}(\tilde{\mathbf{R}})$ . When substituted into Eq. (11) this results in

$$\dot{\tilde{\mathbf{R}}} = -\mu \frac{\tau T_s}{l_0^2} \tilde{\nabla}S_{\text{ex}}(\tilde{\mathbf{R}}) + \tilde{\boldsymbol{\eta}}(\tilde{t}). \quad (14)$$

We conclude from Eq. (10) and Eq. (14) that the reduced AOUP equation of motion is invariant upon a density change if  $\tau D/l_0^2$  and  $\tau T_s/l_0^2$  do not vary. This implies  $D(\rho) \propto T_s(\rho)$  and  $\tau(\rho) \propto \rho^{-2/3}/T_s(\rho)$  in which  $T_s(\rho)$  is short-hand notation for  $T_{\text{eq}}(\rho, S_{\text{ex}}(\tilde{\mathbf{R}}))$ , compare Eq. (13). Working from the reference state point  $(\rho_0, D_0, \tau_0)$ , this means that the function  $T_s(\rho)$  determines how to scale  $D$  and  $\tau$  to ensure invariant AOUP dynamics,

$$\begin{aligned} D(\rho) &= D(\rho_0) \frac{T_s(\rho)}{T_s(\rho_0)} \\ \tau(\rho) &= \tau(\rho_0) \left(\frac{\rho_0}{\rho}\right)^{2/3} \frac{T_s(\rho_0)}{T_s(\rho)}. \end{aligned} \quad (15)$$

We next link to the configurational temperature. There is no reason to expect  $T_{\text{conf}} = T_s$ , and these quantities indeed differ by up to a factor of six in our simulations. However, Eq. (15) still applies with  $T_{\text{conf}}$  instead of  $T_s$  if the two temperatures are proportional in their density variation. To show this we note that Eq. (8) implies  $\tilde{\nabla}U(\mathbf{R}) = T_s \tilde{\nabla}S_{\text{ex}}(\tilde{\mathbf{R}})$  and  $\tilde{\nabla}^2U(\mathbf{R}) = T_s \tilde{\nabla}^2S_{\text{ex}}(\tilde{\mathbf{R}})$ , so  $T_{\text{conf}}(\mathbf{R}) = (\nabla U(\mathbf{R}))^2/\nabla^2U(\mathbf{R}) = (\tilde{\nabla}U(\mathbf{R}))^2/\tilde{\nabla}^2U(\mathbf{R}) = T_s (\tilde{\nabla}S_{\text{ex}}(\tilde{\mathbf{R}}))^2/\tilde{\nabla}^2S_{\text{ex}}(\tilde{\mathbf{R}})$  [50]. Here we ignored the dependence of  $T_s(\mathbf{R})$  on the configuration  $\mathbf{R}$  at a given state point which, as argued above, vanishes in the thermodynamic limit. In terms of  $\phi(\tilde{\mathbf{R}}) \equiv (\tilde{\nabla}S_{\text{ex}}(\tilde{\mathbf{R}}))^2/\tilde{\nabla}^2S_{\text{ex}}(\tilde{\mathbf{R}})$  we thus have

$$\frac{T_{\text{conf}}(\mathbf{R})}{T_{\text{conf}}(\mathbf{R}_0)} = \frac{T_s(\rho) \phi(\tilde{\mathbf{R}})}{T_s(\rho_0) \phi(\tilde{\mathbf{R}}_0)}. \quad (16)$$

Since  $\tilde{\mathbf{R}} = \tilde{\mathbf{R}}_0$  this implies  $T_{\text{conf}}(\mathbf{R})/T_{\text{conf}}(\mathbf{R}_0) = T_s(\rho)/T_s(\rho_0)$ . In this way Eq. (15) leads to Eq. (4). Note that by using  $T_{\text{conf}}$  rather than  $T_s$ , one does not have to identify the equilibrium state point with the same potential energy as the active-matter state point in question.

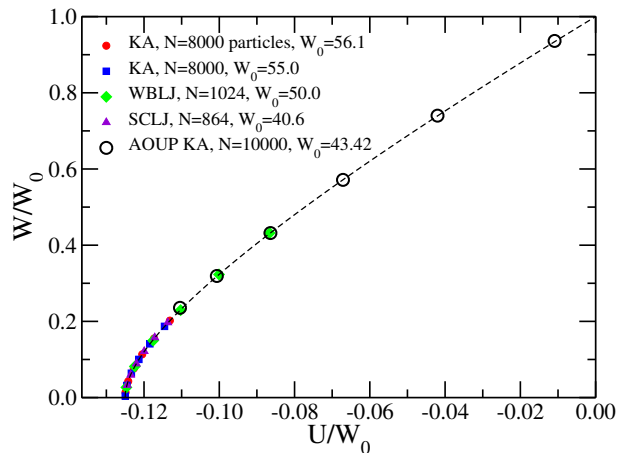


FIG. 4. Master isomorph (dashed curve, Eq. (17)) expressing the virial  $W$  as a function of the potential energy  $U$  for LJ systems along any isomorph;  $W_0$  is the virial at the state point of zero potential energy on the isomorph. This is Fig. 8 of Ref. 51 to which we have added points for the AOUP KA model (open circles). The abbreviations KA, WBLJ, SCLJ stand for the Kob-Andersen system, the Wahnstrom binary LJ mixture [52], and the standard single-component LJ system.

As mentioned, lines of invariance are termed isomorphs in the case of standard Newtonian equilibrium dynamics. This concept was recently generalized to out-of-equilibrium Newtonian systems like that of a shear flow or an aging glass, leading to the introduction of the systemic temperature (Eq. (12)); the name “systemic isomorph” was introduced for the lines of approximately invariant structure and dynamics of the relevant phase diagram [50]. The

results of the present paper demonstrate the existence of systemic isomorphs for non-time-reversible systems like active matter.

We end this section by checking a consequence of the above. It was shown in Ref. 51 for LJ systems that if  $W_0$  is the virial at zero potential energy of a given isomorph, the following relation between the virial  $W$  and the potential energy  $U$  applies along the isomorph in question

$$2 \frac{W}{W_0} = 1 + 8 \frac{U}{W_0} + \sqrt{1 + 8 \frac{U}{W_0}}. \quad (17)$$

This identity is solely a consequence of the reduced-unit RDF isomorph invariance that applies in the R-simple region (liquid or solid, not gas) of any single- or multicomponent LJ system [51]. Since the reduced RDF is also invariant to a good approximation along the above studied KA active-matter systemic isomorph (Fig. 1),  $W$  should also in this case be related to  $U$  according to Eq. (17). This is validated in Fig. 4 that reproduces the Newtonian-dynamics equilibrium data of Ref. 51. It is clear from Fig. 4 that the states considered in the present paper are qualitatively different from the equilibrium states represented in the figure; basically the active systems are dense and corresponds to high-temperature equilibrium fluids.

#### IV. THE YUKAWA ACTIVE BROWNIAN-PARTICLE MODEL IN TWO DIMENSIONS

In order to illustrate the generality of the procedure, this section illustrates the procedure for generating lines of approximately invariant structure and dynamics – systemic isomorphs – for a different active-matter model. We study the active Brownian-particle (ABP) model in two dimensions of the single-component Yukawa pair potential [53, 54]

$$v(r) = \frac{Q^2 \sigma}{r} e^{-r/(\lambda\sigma)}. \quad (18)$$

The Yukawa pair potential has hidden scale invariance [49], so the above developed procedure should apply here as well.

If  $\mathbf{r}_i$  is the position vector of particle  $i$ , the ABP equations of motion in two dimensions is

$$\dot{\mathbf{r}}_i = \mu \mathbf{F}_i + \boldsymbol{\xi}_i(t) + v_0 \mathbf{o}_i(t). \quad (19)$$

Here,  $\mu$  is again the mobility,  $\mathbf{F}_i(\mathbf{R}) = -\nabla_i U(\mathbf{R})$  is the force on particle  $i$ ,  $\boldsymbol{\xi}_i(t)$  is a Gaussian random white-noise vector,  $v_0$  is a constant velocity, and  $\mathbf{o}_i(t) = (\cos(\theta_i(t)), \sin(\theta_i(t)))$  is a stochastic unit vector. The direction vector angle  $\theta_i(t)$  is determined by a white Gaussian noise of magnitude  $D_r$ ,

$$\langle \dot{\theta}_i(t) \dot{\theta}_j(t') \rangle = 2D_r \delta_{ij} \delta(t - t'), \quad (20)$$

and the white-noise vector has magnitude  $D_t$ ,

$$\langle \boldsymbol{\xi}_i^\alpha(t) \boldsymbol{\xi}_j^\beta(t') \rangle = 2D_t \delta_{ij} \delta_{\alpha\beta} \delta(t - t'). \quad (21)$$

The ABP model has four parameter. Regarding again  $\mu$  as a material constant, in order to have invariant physics the dimensionless versions of the three other parameters are required to be constant when the density is changed. Following the procedure of Sec. III we take as units  $l_0 = \rho^{-1/2}$  (the exponent is  $-1/2$  because the model is two-dimensional) and  $t_0 = 1/D_r$ , and write the equation of motion in terms of the corresponding reduced variables. Substituting  $\mathbf{r}_i = \rho^{-1/2} \tilde{\mathbf{r}}_i$  and  $t = (1/D_r) \tilde{t}$  into Eq. (19) and making use of Eq. (8) as well as the definition of the systemic temperature  $T_s$  (Eq. (13)), we get

$$\dot{\tilde{\mathbf{r}}}_i = -\mu \rho (T_s/D_r) \tilde{\nabla}_i S_{\text{ex}}(\tilde{\mathbf{R}}) + \tilde{\boldsymbol{\xi}}_i(t) + \tilde{v}_0 \mathbf{o}_i(t). \quad (22)$$

Here  $\tilde{v}_0 = (\rho^{1/2}/D_r)v_0$ ,  $\tilde{\boldsymbol{\xi}}_i = (\rho^{1/2}/D_r)\boldsymbol{\xi}_i$ ,

$$\langle \tilde{\boldsymbol{\xi}}_i^\alpha(t) \tilde{\boldsymbol{\xi}}_j^\beta(t') \rangle = 2\rho (D_t/D_r) \delta_{ij} \delta_{\alpha\beta} \delta(\tilde{t} - \tilde{t}'), \quad (23)$$

and (with a dot denoting the derivative with respect to  $\tilde{t}$ )

$$\langle \dot{\theta}_i(t) \dot{\theta}_j(t') \rangle = 2\delta_{ij} \delta(\tilde{t} - \tilde{t}'). \quad (24)$$

These equations are invariant under a change of density if  $\mu\rho T_s/D_r$ ,  $\rho D_t/D_r$ , and  $\tilde{v}_0$  are all constant. Since  $\mu$  is a material constant, this implies (where the subscript zero refers to a reference state of density  $\rho_0$  and  $T_s(\rho) \equiv T_{\text{eq}}(\rho, S_{\text{ex}}(\tilde{\mathbf{R}}))$ )

$$\begin{aligned} D_r &= D_{r,0} \frac{\rho}{\rho_0} \frac{T_s(\rho)}{T_s(\rho_0)} \\ D_t &= D_{t,0} \frac{T_s(\rho)}{T_s(\rho_0)} \\ v_0 &= v_{0,0} \left( \frac{\rho}{\rho_0} \right)^{1/2} \frac{T_s(\rho)}{T_s(\rho_0)}. \end{aligned} \quad (25)$$

By the same argument as in Sec. III one can here replace  $T_s(\rho)$  by  $T_{\text{conf}}(\mathbf{R})$ , leading to

$$\begin{aligned} D_r &= D_{r,0} \frac{\rho}{\rho_0} \frac{T_{\text{conf}}[(\rho_0/\rho)^{1/2}\mathbf{R}_0]}{T_{\text{conf}}(\mathbf{R}_0)} \\ D_t &= D_{t,0} \frac{T_{\text{conf}}[(\rho_0/\rho)^{1/2}\mathbf{R}_0]}{T_{\text{conf}}(\mathbf{R}_0)} \\ v_0 &= v_{0,0} \left( \frac{\rho}{\rho_0} \right)^{1/2} \frac{T_{\text{conf}}[(\rho_0/\rho)^{1/2}\mathbf{R}_0]}{T_{\text{conf}}(\mathbf{R}_0)}. \end{aligned} \quad (26)$$

We note in passing that while the Peclet number  $v_0/\sqrt{2D_r D_t}$  [16, 55] is invariant along the systemic isomorph, requiring this is not enough to determine how to scale the model parameters; thus Peclet-number invariance is a necessary but not sufficient condition for identifying a systemic isomorph. For certain systems of ABPs the ratio of  $D_r$  and  $D_t$  is fixed (e.g., by the size of the colloidal sphere). This may bring into question the relevance of the above transformation, but even for such systems Eq. (26) may be used for comparing state points of different models.

$\rho$	$D_r$	$D_t$	$v_0$	$T_{\text{conf}}$
1.0	3.000	1.000	25.00	1.489
1.5	12.37	2.750	84.20	4.093
2.0	30.43	5.072	179.3	7.550
2.5	58.13	7.751	306.4	11.54
3.0	95.82	10.65	461.0	15.85

TABLE II. Values of  $\rho$ ,  $D_r$ ,  $D_t$ ,  $v_0$ , and  $T_{\text{conf}}$  along the systemic isomorph. As in Table I,  $T_{\text{conf}}(\rho)$  is determined from a single configuration  $\mathbf{R}_0$  by means of Eq. (1).

To validate the above prediction we simulated  $N = 10000$  particles of the 2d Yukawa system with  $Q = 50$ ,  $\lambda = 0.16$ ,  $\sigma = 1$  defining the length unit, and a cutoff at  $4.5\sigma$ . The time step used is given by  $\Delta t = \Delta\tilde{t}(D_t/v_0^2)$ , where  $\Delta\tilde{t} = 0.0625$  so that  $\Delta t = 0.0001$  at the reference state point defined by  $(\rho, D_r, D_t, v_0) = (1.0, 3.0, 1.0, 25.0)$ . All simulations were carried out on GPU cards using a home-made code. A systemic isomorph was traced out for densities varying a factor of three using Eq. (26) for a configuration  $\mathbf{R}_0$  selected from a simulation at the reference state point. Table II gives the parameters obtained from Eq. (26).

Figure 5(a) shows the radial distribution function (RDF). The left two panels show the RDF along the systemic isomorph as a function of  $r$  and  $\tilde{r}$ , respectively, while the right panel for comparison shows the results for the same parameters at the reference state-point density  $\rho = 1.0$ . We find a good invariance of the reduced-unit RDF along the systemic isomorph. The same is the case for the reduced-unit MSD shown in the middle panel of (b); the left panel gives the MSD as a function of time while the right panel for comparison is the reduced-unit MSD along the  $\rho = 1.0$  isochore.

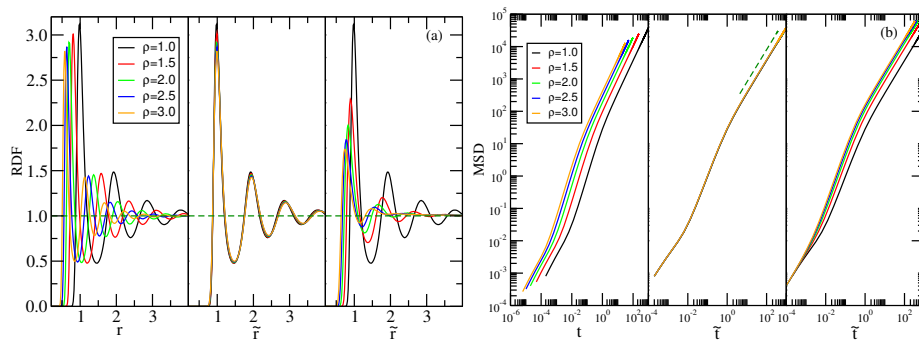


FIG. 5. Structure and dynamics of the Yukawa ABP model in two dimensions. (a) The left panel shows the RDF as a function of the pair distance  $r$  along the systemic isomorph, the middle panel shows the same data in reduced units, and the right panel shows the RDF for the same parameters (Table II) at the reference density  $\rho = 1.0$ . (b) The left panel shows the MSD as a function of time  $t$  along the systemic isomorph, the middle panel shows the same data in reduced units where the dashed lines mark slope unity (ordinary diffusion), and the right panel shows the MSD for the same parameters at the reference density.

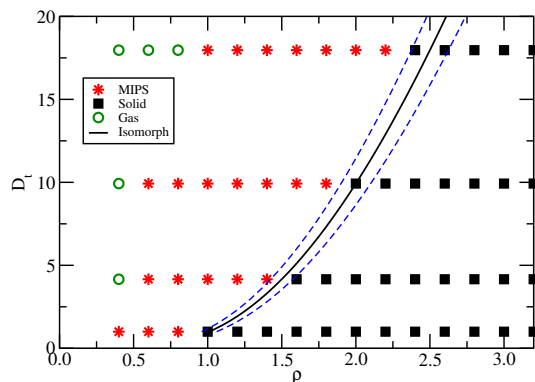


FIG. 6. Phase diagrams showing MIPS state points as red stars and homogeneous state points as black squares; green circles are gas-like states. The MIPS phase consists of coexisting phases that differ by the density, the denser of which corresponds to the “solid” homogeneous phase that consists of hexagonal solid crystals. The reference state point  $(\rho, D_r, D_t, v_0) = (1.01, 3, 1, 367)$  is located in the homogeneous (solid) phase close to the phase boundary. From it a systemic isomorph has been traced out using Eq. (26) (black line). The figure gives data in the  $(\rho, D_t)$  phase diagram with  $D_r$  and  $v_0$  given by Eq. (26) at density  $\rho$ . The blue dashed line marks  $\pm 5\%$  variations in density.

## V. THE MIPS BOUNDARY OF THE 2D ABP YUKAWA MODEL

The 2d ABP Yukawa model is a model for which motility-induced phase separation (MIPS) appears for certain parameter choices. Identifying which constants lead to MIPS and which do not may be tedious because the phase diagram is four dimensional. We show in this section that the configurational-temperature provides a method for reducing the number of simulations needed to map out the phase diagram. The idea is that, because the physics is approximately invariant along a systemic isomorph, this cannot cross the MIPS boundary. Thus if one has identified a state point in the homogeneous solid phase that is close to the MIPS boundary and use this as reference state point, all state points identified by Eq. (26) should also be close to the MIPS boundary. A similar line of reasoning has been validated for the melting line of the standard Lennard-Jones system [56].

To investigate this use of the configurational temperature, we studied the Yukawa model with parameters  $Q = 1000$  and  $\lambda = 0.12$  with a cutoff at  $4.2\sigma$ . We then fixed the model parameters to the values  $(D_r, D_t, v_0) = (3, 1, 367)$  and systematically decreased the density from a high value where one is well within the homogeneous solid phase. A system of 40000 particles was simulated for 40 million time steps and the occurrence of MIPS was detected by visual inspection (subsequent simulations involved just 10000 particles). The lowest density before observing MIPS was  $\rho = 1.01$ . We then used  $(\rho, D_r, D_t, v_0) = (1.01, 3, 1, 367)$  as reference state point for generating a systemic isomorph according to Eq. (26). This is the black full line in Fig. 7, which shows the results of investigating the existence of MIPS in a  $(\rho, D_t)$  phase diagram where the parameters  $D_r(\rho)$ ,  $D_t(\rho)$ , and  $v_0(\rho)$  are given by Eq. (26). The black squares denote state points of the homogeneous solid phase, the red stars denote state points where MIPS appears

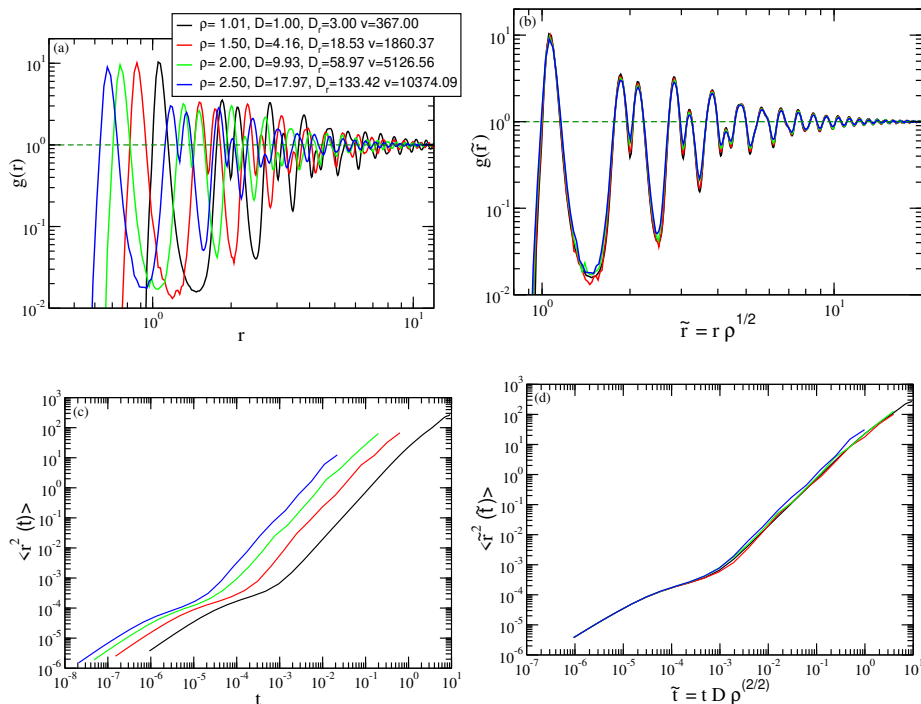


FIG. 7. Structure and dynamics probed along the MIPS phase boundary of the 2d ABP Yukawa system, slightly into the homogeneous phase (compare Fig. 6). The left figures (a) and (c) show the radial distribution function and the mean-square displacement, respectively, and the right figures (b) and (d) show the same data in reduced units. The reduced-unit physics is invariant to a good approximation along the boundary, confirming that it is a close to being a systemic isomorph.

(the low-density green circles denote gas-phase state points). The blue dashed lines mark the systemic isomorph  $\pm 5\%$  in density. We see that the phase transition line is predicted well though not entirely accurately; this is consistent with the approximate nature of the argument. Nevertheless, the simulations demonstrate that Eq. (26) can be used to help in identifying the MIPS phase by significantly reducing the required number of simulations.

In order to validate that the black line of Fig. 7 is indeed a line of approximately invariant physics we show in Fig. 7 how structure and dynamics vary along it. The left figures show the RDF and MSD in standard units while the right figures show the same data in reduced units.

## VI. HOW FAR IS A GIVEN ACTIVE-MATTER SYSTEM FROM EQUILIBRIUM?

We have shown that, despite the fact that its justification is based on the canonical ensemble of equilibrium statistical mechanics, the configurational temperature  $T_{\text{conf}}$  may be used for predicting lines of approximately invariant physics of certain active-matter models of particles without orientational interactions. In contrast to other temperatures discussed in connection with active matter, the use of  $T_{\text{conf}}$  does not embody a mapping to equilibrium.

We end the paper by suggesting a further application of  $T_{\text{conf}}$ , namely that it may be used for quantifying how far an active matter system is from ordinary thermal equilibrium. In the context of ordinary non-active matter researchers have introduced thermostats based on the idea of configurational temperature and used them in the context of non-equilibrium simulations [2], but the application proposed below is simpler and does not involve any thermostat. Quantifying the degree of non-equilibrium is often done by calculating one or the other form of entropy production, which is zero in thermal equilibrium and thus provides a measure of how far a system is from equilibrium [22, 30, 33]. However, using a quantity that goes to zero in some limit to quantify the degree of deviation from that limit does not in any obvious way make it possible to identify when deviations from equilibrium are to be regarded as “large”. If deviations from equilibrium are instead quantified by means of a quantity that goes to unity in the equilibrium limit, deviations from equilibrium can be regarded as “small” whenever that quantity does not deviate substantially from unity.

To illustrate this, we have performed simulations of the 2d ABP Yukawa model at different values of the constant velocity  $v_0$ . Figure 8(a) shows the systemic temperature  $T_s$  and the configurational temperature  $T_{\text{conf}}$  as functions of

$v_0$  for fixed values of the remaining three model parameters; here  $T_s$  was determined numerically by identifying the equilibrium temperature at which the system under a MD simulation has the same average potential energy as the active-matter system in question. Both  $T_s$  and  $T_{\text{conf}}$  converge to 2 as  $v_0 \rightarrow 0$ , which is the equilibrium Brownian-dynamics temperature ( $D_t = 2$ ,  $\mu = 1$ ). Figure 8(b) shows the dissipated “active” power, i.e., the average of the dot product of the particle velocity with the  $v_0$  term of Eq. (19). The proposal is now to quantify the deviation from equilibrium in terms of the ratio  $T_s/T_{\text{conf}}$ , and Fig. 8(c) plots the dissipated power against this ratio. We here also included data where the power is given in isomorph-reduced units (red points), which interestingly show an almost linear dependence on  $T_s/T_{\text{conf}}$ . Figure 8(d) shows  $\log(\text{Power})$  versus  $T_s/T_{\text{conf}}$ . From these simulations one would conclude that the active matter system starts to deviate substantially from an equilibrium system when  $v_0$  is larger than about 3 because here  $T_s/T_{\text{conf}}$  is roughly 1.1.

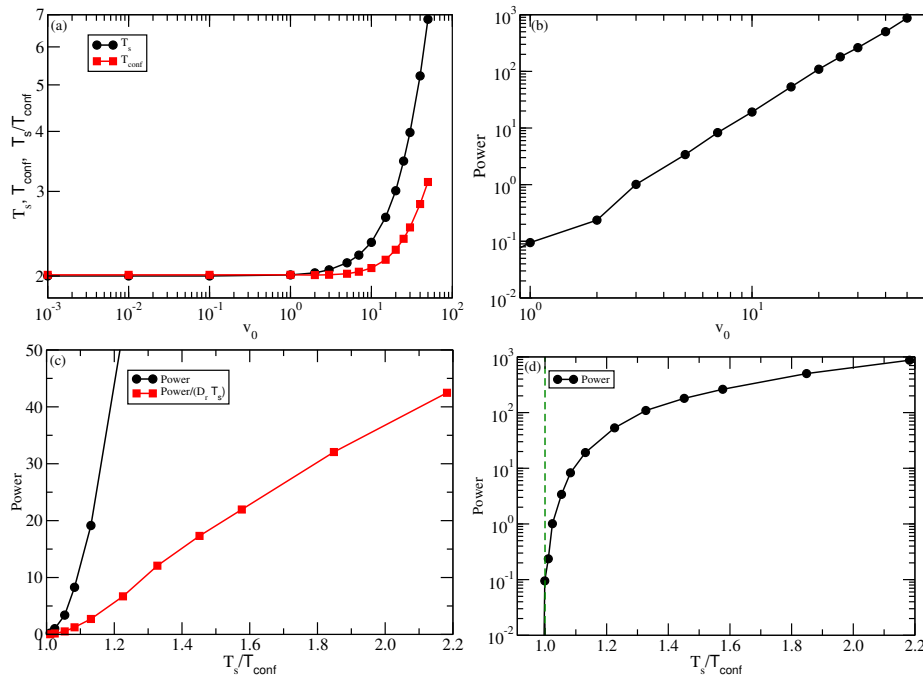


FIG. 8. Using the configurational temperature to quantify how far the system is from thermal equilibrium, corresponding to  $v_0 = 0$  in Eq. (19); the parameters used here are  $\rho = 1$ ,  $D_r = 3$ , and  $D_t = 2$ . (a) and (b) show how the systemic temperature  $T_s$  and the configurational temperature  $T_{\text{conf}}$  vary with  $v_0$  (left) and how the dissipation (Power) in MD units varies with  $v_0$  (right). From (a) we see that when  $v_0 \rightarrow 0$ , the two temperatures become identical (equal to 2 because  $D_t = 2$  and  $D_t$  corresponds to the equilibrium temperature); at the same time the dissipation goes to zero (b). (c) and (d) show the Power as a function of  $T_s/T_{\text{conf}}$ . The quantity  $T_s/T_{\text{conf}}$  goes to unity as thermal equilibrium is approached, which presents an advantage compared to using the dissipated Power for quantifying deviations from equilibrium.

## VII. OUTLOOK

Active-matter models involve more parameters than conventional equilibrium models. We have shown that the configurational temperature provides a tool for reducing significantly the amount of simulations needed to get an overview of the phase diagram. If the pair potential is known for an experimental system, the same method may be useful for obtaining information about regions of the phase diagram that are not easily accessible. Unfortunately, the method is limited to models based on a potential-energy function with hidden scale invariance, but fortunately this constitutes a fairly large class that includes, e.g., Mie-type pair potentials and the Yukawa pair potential. Mixing two and three components, even considering broad polydisperse mixtures, does not ruin the hidden-scale-invariance property [37]. It is our hope that  $T_{\text{conf}}$  besides its ability to identify systemic isomorphs may also turn out to be useful for clarifying some of the puzzles of active matter, for instance the recently discovered non-trivial dependence of the apparent glass transition on the persistence time [57]. More generally, since the above reasoning is not dependent on specific properties of active matter, the configurational temperature may also turn out to be useful in other out-of-equilibrium situations, for instance that of a nonlinear flow or of physical aging.

## ACKNOWLEDGMENTS

This work was supported by the VILLUM Foundation's *Matter* grant (16515).

- 
- [1] J. Casas-Vazquez and D. Jou, "Temperature in non-equilibrium states: a review of open problems and current proposals," *Rep. Prog. Phys.* **66**, 1937–2023 (2003).
- [2] J. G. Powles, G. Rickayzen, and D. M. Heyes, "Temperatures: old, new and middle aged," *Mol. Phys.* **103**, 1361–1373 (2005).
- [3] L. Leuzzi, "A stroll among effective temperatures in aging systems: Limits and perspectives," *J. Non-Cryst. Solids* **355**, 686–693 (2009).
- [4] A. Puglisi, A. Sarracino, and A. Vulpiani, "Temperature in and out of equilibrium: A review of concepts, tools and attempts," *Phys. Rep.* **709-710**, 1–60 (2017).
- [5] D. Zhang, X. Zheng, and M. Di Ventura, "Local temperatures out of equilibrium," *Phys. Rep.* **830**, 1–66 (2019).
- [6] L. F. Cugliandolo and J. Kurchan, "On the out-of-equilibrium relaxation of the Sherrington-Kirkpatrick model," *J. Phys. A: Math. Gen.* **27**, 5749–5772 (1994).
- [7] L. F. Cugliandolo, "The effective temperature," *J. Phys. A: Mathematical and Theoretical* **44**, 483001 (2011).
- [8] I. Petrelli, L. F. Cugliandolo, G. Gonnella, and A. Suma, "Effective temperatures in inhomogeneous passive and active bidimensional Brownian particle systems," *Phys. Rev. E* **102**, 012609 (2020).
- [9] A. Q. Tool, "Relation between inelastic deformability and thermal expansion of glass in its annealing range," *J. Amer. Ceram. Soc.* **29**, 240–253 (1946).
- [10] G. W. Scherer, *Relaxation in Glass and Composites* (Wiley, New York, 1986).
- [11] L. D. Landau and E. M. Lifshitz, *Statistical Physics* [Eq. (33.14)] (Pergamon, Oxford, 1958).
- [12] H. H. Rugh, "Dynamical approach to temperature," *Phys. Rev. Lett.* **78**, 772–774 (1997).
- [13] M. Himpel and A. Melzer, "Configurational temperature in dusty plasmas," *Phys. Rev. E* **99**, 063203 (2019).
- [14] T. E. Angelini, E. Hannezo, X. Trepát, M. Marquez, J. J. Fredberg, and D. A. Weitz, "Glass-like dynamics of collective cell migration," *Proc. Natl. Acad. Sci. (USA)* **108**, 4714–4719 (2011).
- [15] M. C. Marchetti, J. F. Joanny, S. Ramaswamy, T. B. Liverpool, J. Prost, M. Rao, and R. A. Simha, "Hydrodynamics of soft active matter," *Rev. Mod. Phys.* **85**, 1143–1189 (2013).
- [16] C. Bechinger, R. Di Leonardo, H. Löwen, C. Reichhardt, G. Volpe, and G. Volpe, "Active particles in complex and crowded environments," *Rev. Mod. Phys.* **88**, 045006 (2016).
- [17] S. Ramaswamy, "Active matter," *J. Stat. Mech.* , 054002 (2017).
- [18] D. Saintillan, "Rheology of active fluids," *Annu. Rev. Fluid Mech.* **50**, 563–592 (2018).
- [19] M. Das, C. F. Schmidt, and M. Murrell, "Introduction to active matter," *Soft Matter* **16**, 7185–7190 (2020).
- [20] M. R. Shaebani, A. Wysocki, R. G. Winkler, G. Gompper, and H. Rieger, "Computational models for active matter," *Nat. Rev. Phys.* **2**, 181–199 (2021).
- [21] M. J. Bowick, N. Fakhri, C. M. Marchetti, and S. Ramaswamy, "Symmetry, thermodynamics, and topology in active matter," *Phys. Rev. X* **12**, 010501 (2022).
- [22] J. O'Byrne, Y. Kafri, J. Tailleur, and F. van Wijland, "Time irreversibility in active matter, from micro to macro," *Nat. Rev. Phys.* **4**, 167–183 (2022).
- [23] R. Mandal, P. J. Bhuyan, P. Chaudhuri, C. Dasgupta, and M. Rao, "Extreme active matter at high densities," *Nat. Comm.* **11**, 2581 (2020).
- [24] T. Vicsek, A. Czirók, E. Ben-Jacob, I. Cohen, and O. Shochet, "Novel type of phase transition in a system of self-driven particles," *Phys. Rev. Lett.* **75**, 1226–1229 (1995).
- [25] S. K. Das, S. A. Egorov, B. Trefz, P. Virnau, and K. Binder, "Phase behavior of active swimmers in depletants: Molecular dynamics and integral equation theory," *Phys. Rev. Lett.* **112**, 198301 (2014).
- [26] M. E. Cates and J. Tailleur, "Motility-induced phase separation," *Ann. Rev. Cond. Mat. Phys.* **6**, 219–244 (2015).
- [27] D. Geyer, D. Martin, J. Tailleur, and D. Bartolo, "Freezing a flock: Motility-induced phase separation in polar active liquids," *Phys. Rev. X* **9**, 031043 (2019).
- [28] C. Merrigan, K. Ramola, R. Chatterjee, N. Segall, Y. Shokef, and B. Chakraborty, "Arrested states in persistent active matter: Gelation without attraction," *Phys. Rev. Research* **2**, 013260 (2020).
- [29] G. Szamel, "Self-propelled particle in an external potential: Existence of an effective temperature," *Phys. Rev. E* **90**, 012111 (2014).
- [30] E. Fodor, C. Nardini, M. E. Cates, J. Tailleur, P. Visco, and F. van Wijland, "How far from equilibrium is active matter?" *Phys. Rev. Lett.* **117**, 038103 (2016).
- [31] D. Loi, S. Mossa, and L. F. Cugliandolo, "Effective temperature of active matter," *Phys. Rev. E* **77**, 051111 (2008).
- [32] S. Wang and P. G. Wolynes, "Communication: Effective temperature and glassy dynamics of active matter," *J. Chem. Phys.* **135**, 051101 (2011).
- [33] E. Flenner and G. Szamel, "Active matter: Quantifying the departure from equilibrium," *Phys. Rev. E* **102**, 022607 (2020).
- [34] S. C. Takatori and J. F. Brady, "Towards a thermodynamics of active matter," *Phys. Rev. E* **91**, 032117 (2015).

- [35] N. Gnan, T. B. Schröder, U. R. Pedersen, N. P. Bailey, and J. C. Dyre, “Pressure-energy correlations in liquids. IV. “Isomorphs” in liquid phase diagrams,” *J. Chem. Phys.* **131**, 234504 (2009).
- [36] T. B. Schröder and J. C. Dyre, “Simplicity of condensed matter at its core: Generic definition of a Roskilde-simple system,” *J. Chem. Phys.* **141**, 204502 (2014).
- [37] T. S. Ingebrigtsen and H. Tanaka, “Effect of size polydispersity on the nature of Lennard-Jones liquids,” *J. Phys. Chem. B* **119**, 11052–11062 (2015).
- [38] J. C. Dyre, “Perspective: Excess-entropy scaling,” *J. Chem. Phys.* **149**, 210901 (2018).
- [39] W. Kob and H. C. Andersen, “Testing mode-coupling theory for a supercooled binary Lennard-Jones mixture I: The van Hove correlation function,” *Phys. Rev. E* **51**, 4626–4641 (1995).
- [40] T. S. Ingebrigtsen, J. C. Dyre, T. B. Schröder, and C. P. Royall, “Crystallization instability in glass-forming mixtures,” *Phys. Rev. X* **9**, 031016 (2019).
- [41] S. Toxvaerd and J. C. Dyre, “Communication: Shifted forces in molecular dynamics,” *J. Chem. Phys.* **134**, 081102 (2011).
- [42] N. P. Bailey, T. S. Ingebrigtsen, J. S. Hansen, A. A. Veldhorst, L. Bøhling, C. A. Lemarchand, A. E. Olsen, A. K. Bacher, L. Costigliola, U. R. Pedersen, H. Larsen, J. C. Dyre, and T. B. Schröder, “RUMD: A general purpose molecular dynamics package optimized to utilize GPU hardware down to a few thousand particles,” *Scipost Phys.* **3**, 038 (2017).
- [43] Y. Fily, Y. Kafri, A. P. Solon, J. Tailleur, and A. Turner, “Mechanical pressure and momentum conservation in dry active matter,” *J. Phys. A* **51**, 044003 (2017).
- [44] T. F. F. Farage, P. Krinninger, and J. M. Brader, “Effective interactions in active Brownian suspensions,” *Phys. Rev. E* **91**, 042310 (2015).
- [45] C. Maggi, U. M. B. Marconi, N. Gnan, and R. DiLeonardo, “Multidimensional stationary probability distribution for interacting active particles,” *Sci. Rep.* **5**, 10742 (2015).
- [46] G. Szamel, E. Flenner, and L. Berthier, “Glassy dynamics of athermal self-propelled particles: Computer simulations and a nonequilibrium microscopic theory,” *Phys. Rev. E* **91**, 062304 (2015).
- [47] J.-P. Hansen and I. R. McDonald, *Theory of Simple Liquids: With Applications to Soft Matter*, 4th ed. (Academic, New York, 2013).
- [48] J. C. Dyre, “Hidden scale envariance in condensed matter,” *J. Phys. Chem. B* **118**, 10007–10024 (2014).
- [49] A. A. Veldhorst, T. B. Schröder, and J. C. Dyre, “Invariants in the Yukawa system’s thermodynamic phase diagram,” *Phys. Plasmas* **22**, 073705 (2015).
- [50] J. C. Dyre, “Isomorph theory beyond thermal equilibrium,” *J. Chem. Phys.* **153**, 134502 (2020).
- [51] T. B. Schröder, N. Gnan, U. R. Pedersen, N. P. Bailey, and J. C. Dyre, “Pressure-energy correlations in liquids. V. Isomorphs in generalized Lennard-Jones systems,” *J. Chem. Phys.* **134**, 164505 (2011).
- [52] G. Wahnström, “Molecular-dynamics study of a supercooled two-component Lennard-Jones system,” *Phys. Rev. A* **44**, 3752 (1991).
- [53] H. Yukawa, “On the interaction of elementary particles,” *Proc. Phys.-Math. Soc. Jpn.* **17**, 48–57 (1935).
- [54] O. J. Meacock, A. Doostmohammadi, K. R. Foster, J. M. Yeomans, and W. M. Durham, “Bacteria solve the problem of crowding by moving slowly,” *Nat. Phys.* **17**, 205–210 (2021).
- [55] L. Hecht, J. C. Urena, and B. Liebchen, “An introduction to modeling approaches of active matter,” *arXiv*, 2102.13007 (2021).
- [56] L. Costigliola, T. B. Schröder, and J. C. Dyre, “Freezing and melting line invariants of the Lennard-Jones system,” *Phys. Chem. Chem. Phys.* **18**, 14678 – 14690 (2016).
- [57] L. Berthier, E. Flenner, and G. Szamel, “How active forces influence nonequilibrium glass transitions,” *New J. Phys.* **19**, 125006 (2017).